Journal of Engineering Mathematics **29:** 557–574, 1995.

A dynamic simulation of the conforming shell gas journal bearing

S. D. HOWISON[1], D. F. MAYERS[2] and W. R. SMITH[3]
[1]*Mathematics Institute, 24–29 St. Giles, Oxford, U.K.*
[2]*Computing Laboratory, 8–11 Keble Road, Oxford, U.K.*
[3]*Fluid Gravity (Eng) Ltd, Chiltlee Manor, Haslemere Road, Liphook, Hampshire, U.K.*

Received 7 March 1994; accepted in revised form 8 February 1995

Abstract. A time-dependent mathematical model for the conforming shell gas journal bearing is presented. A numerical scheme is devised to solve this mathematical model. The results of a dynamic simulation of the bearing are exhibited for a specific design.

1. Introduction

This article is devoted to the study of the conforming shell gas journal bearing, which is a potentially attractive alternative to roller bearings in gas turbine applications. It is expected to operate at higher shaft speeds and operating temperatures, and in addition the shell system can deform to accept higher loads than conventional gas bearings. Furthermore, it does not require the pressurisation systems of a conventional oil-lubricated bearing.

A typical bearing, sketched in Fig. 1, consists of a rigid journal surrounded by flexible shells or pads. The journal rotates about a movable axis called the *shaft centre*. The shells are supported by flexible bridge pieces generally referred to as springs. Hemispherical joints connect each spring to a fixed housing. These hemispherical joints allow the springs to pivot.

The shells overlap each other at their leading and trailing edges. The trailing edge of the lagging shell is always closer to the journal than the leading edge of the leading shell. A specified step height is built into this overlap, so that the trailing edge of the lagging shell is closer to the journal than the leading edge of the leading shell by at least the step height. There is a built-in distance between shells and journal before any component moves or deforms called the *diametric clearance*.

Each spring makes two line contacts with the shells; the leading edge of the spring meets the adjacent shell about half-way from the leading edge of the shell, and the other is between the trailing spring arm and leading edge of the preceding shell.

As the journal rotates, it drags air into the gaps between journal and shells. This generates pressures which cause the shells to deform about the shell-to-spring contacts. The springs also compress and rotate about the hemispherical joint in response to these pressures.

The shaft centre is free to translate within the housing. The pressures generated between the journal and the shells form the only mechanism controlling the motion of the shaft centre. The motion of the journal therefore links the behaviour of all the shells, and a steady state can only be reached when the pressures between shells and journal resolve to equal the applied load on the journal.

In general the shells and springs are all coupled mechanically, but the shells and springs are not connected together. Thus, contact between adjacent shells can be lost and regained in

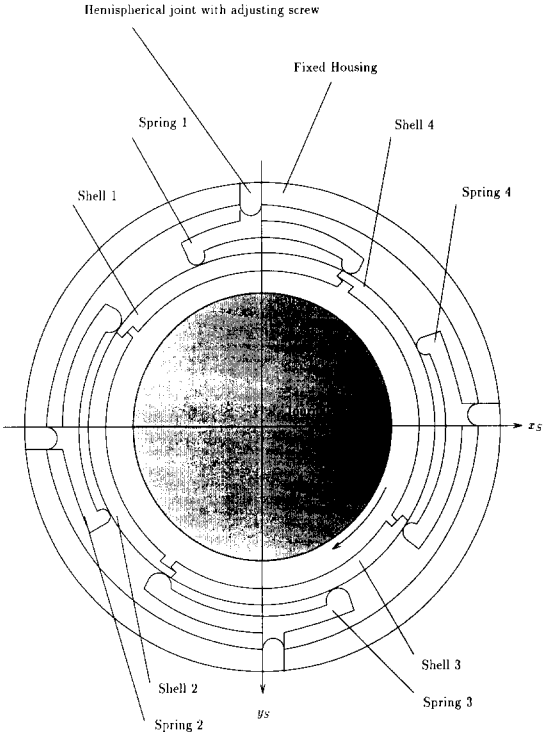

Fig. 1. Conforming shell gas journal bearing.

response to an applied load on the journal. Also a spring can become completely detached from the rest of the bearing and regain contact again. The springs can, however, be considered linked to the rigid housing. There is no reason why several breaks and contacts cannot occur at the same time.

It is important to realise that Fig. 1 is not to scale. The length of the journal-to-shell air gap is much smaller than the circumferential length of the shell. The radial width of the shell is also much smaller than the circumferential length of the shell. The axial length of the shell is comparable to the circumferential length of the shell.

The main objective of this article is to determine the stability of a bearing design. The configuration of shells, springs and shaft at steady state will also be evaluated. Other important points include whether separations can occur and, if so, when. The journal-to-shell air gap cannot be allowed to become arbitrarily small: a minimum air gap of five microns is generally accepted. The minimum film thickness should therefore be determined, especially at steady state.

The accepted method in the engineering literature for finding steady states and stability of complex bearings is the nonlinear orbit method ([1], [2]). This involves the integration of a dynamic model from initial conditions forward in time. Thus, a time-dependent mathematical model is required.

This article is split into five sections. In Section 2, a mathematical model is developed which is sufficiently simple to admit solution techniques, but at the same time accurately represents the bearing. Section 3 deals with the numerical method to solve the model from Section 2. Section 4 is an examination of the results of the simulation. Finally Section 5 briefly draws some conclusions.

2. Mathematical model

The mathematical model incorporates assumptions about the design; these must be physically realistic or the resulting predictions may be inaccurate. The problem is not just to write down equations that represent the bearing, but also to solve these equations. The equations should be simplified as much as possible whilst the model still remains realistic.

The long-thin geometry, typically characterised by an aspect ratio of 10^{-3}, is exploited to make asymptotic reductions of the Navier–Stokes equations. Gas lubricating films are very nearly isothermal because of the ability of the bearing materials to conduct away heat is greater than the heat generating capacity of the gas-film, see [3]. Thus, we assume the flow is isothermal. As gas viscosity is somewhat insensitive to changes in pressure and the temperature is virtually constant, we assume the gas viscosity is constant. Slip flow is negligible when the mean free path of the gas is small compared with the dimensions of the flow passage. The mean free path of the gas is much less than the minimum restriction of five microns placed on the film thickness. In addition, as seen in [4], slip flow effects at high speeds are less important. Thus, we shall assume no-slip conditions. The reduced Reynolds number is typically less than 10^{-4} and therefore negligible in comparison to 1. No discontinuities in pressure or velocity are considered as Mach number is small. The Reynolds equation can be deduced as, for example, in [5]. Bearing surfaces will be assumed to be infinitely long so that only the one-dimensional form of Reynolds' equation need be solved. This assumption neglects the flow of gas in and out of the sides of the bearing (side flow). (An investigation of the influence of two-dimensional effects on the predicted performance of journal bearings is described in [6].)

Let P^i be the pressure on shell i, H^i the film thickness on shell i, T time, X arclength, μ viscosity, U speed of the shaft surface, B a typical arclength, p_a ambient pressure, c a typical film thickness and ν a typical shaft rotation frequency. After the non-dimensionalisation of $X = Bx$, $T = t/\nu$, $H^i = ch^i$ and $P^i = p_a p^i$, the compressible Reynolds equation is given by

$$\sigma \frac{\partial}{\partial t}(p^i h^i) + \Lambda \frac{\partial}{\partial x}(p^i h^i) = \frac{\partial}{\partial x}\left(p^i h^i \frac{\partial p^i}{\partial x}\right), \tag{1}$$

where the bearing number is given by

$$\Lambda = \frac{6\mu U B}{p_a c^2},$$

and the squeeze number by

$$\sigma = \frac{12\mu B^2 \nu}{p_a c^2}.$$

The pressure is assumed to return to ambient at either side of the shell, so the boundary conditions for Reynolds' equation are $p^i(0,t) = 1$ and $p^i(R,t) = 1$ where $R = L/B$. The initial conditions are arbitrary.

The shells are modelled by curved beams [7] as they are long and thin, typically characterised by an aspect ratio of 10^{-2}. The time scales of the shells and springs are typically one hundredth of the time scale appropriate to the fluid motion. Thus, the shells and springs are assumed to have negligible mass and moment inertia. Also the radial distance between the

lower surface of the beam and the centre line is presumed constant, so that these two quantities can be simply related. A delta function is used to model the spring contact which takes place over a relatively small area.

Let W^i be the deformation of the centre line of shell i, F_1^i the spring force radially inward on shell i from the leading edge of spring i, E the Young's modulus, I the moment of inertia of the cross section about an axis through its centroid and perpendicular to the plane of the couple, d the axial length of the shell and R_P the initial radius of the shells. After the non-dimensionalisation $W^i = cw^i$ and $F_1^i = p_a B f_1^i$, the curved beam equation is given by

$$r\left\{\frac{\partial^4 w^i}{\partial x^4} + 2\kappa^2 \frac{\partial^2 w^i}{\partial x^2} + \kappa^4 w^i\right\} = 1 - p^i + f_1^i \delta(x - x'), \tag{2}$$

where

$$r = \frac{EIc}{p_a d B^4}$$

and

$$\kappa = \frac{B}{R_P}.$$

These dimensionless parameters represent non-dimensional measures of flexural rigidity and curvature respectively. The boundary conditions are

$$\left(\frac{\partial^2 w^i}{\partial x^2} + \kappa^2 w^i\right)(0,t) = 0, \qquad \left(\frac{\partial^2 w^i}{\partial x^2} + \kappa^2 w^i\right)(R,t) = 0$$

and

$$w^i(R,t) = 0.$$

Also there is a restriction on the solution space,

$$w^i(x',t) = 0,$$

in which x' is the point of spring contact within the domain $(0, R)$.

The rigid body motion of the shaft is described simply by Newton's second law. Let (X_S, Y_S) be the Cartesian coordinates of the centre of the shaft (Fig. 1), W_L the external load per unit axial length, L the length of the shell, θ the angle measured anticlockwise from the line of action of the applied force and M the shaft mass per unit axial length. After non-dimensionalisation by $X_S = cx_S$ and $Y_S = cy_S$, the resolution equations are written

$$\frac{\mathrm{d}^2 x_S}{\mathrm{d}t^2} = \Gamma \sum_i \int_0^R p^i \sin\theta \, \mathrm{d}x \tag{3}$$

and

$$\frac{\mathrm{d}^2 y_S}{\mathrm{d}t^2} = \Gamma \sum_i \int_0^R p^i \cos\theta \, \mathrm{d}x + l, \tag{4}$$

where $\Gamma = p_a B / M c\nu^2$ and $l = W_L / M c\nu^2$. The initial conditions on X_S, $\dot{X}_S$, Y_S and $\dot{Y}_S$ are prescribed according to the application under consideration.

The remaining physics consists of the geometry and the equilibrium of forces. The movement is decomposed into rigid body motion and elastic deformations. The possible rigid body motions are separated as follows:

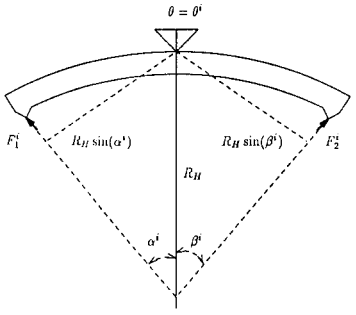

Fig. 2. Spring in a circular geometry.

(a) rigid body motion of the shaft;
(b) rigid body motion of the springs;
(c) rigid body motion of the shells.

The unknowns for these rigid body motions are as follows:

(a) position and velocity of the shaft centre: (x_S, y_S), $(\dot{x}_S, \dot{y}_S)$;
(b) angle of rotation of spring i : ψ^i;
(c) two degrees of freedom for each shell (defined in equation (8)): ξ_t^i, η_t^i.

The modelling of these combined rigid body motions and elastic deformations requires some complicated geometry. Similarly, the equations for equilibrium of the forces on the springs and shells are complicated. The unknown forces per unit axial length are f_0^i, f_1^i, f_2^i and f_3^i. These unknowns are solved for by taking moments for the spring, taking moments for the shell, resolving for the shell and matching forces between shells. The derivations of these equations are included here for completeness.

Consider spring i as in Fig. 2. Let R_H be the radius of the housing, α^i the angle subtended from the leading edge of spring i to the pivot and β^i the angle subtended from the trailing edge of spring i to the pivot. After non-dimensionalisation by $F_1^i = p_a B f_1^i$ and $F_2^i = p_a B f_2^i$, the moment equation for the spring becomes

$$f_1^i \sin(\alpha^i) = f_2^i \sin(\beta^i). \tag{5}$$

The spring is assumed to satisfy Hooke's Law on both sides of the pivot. This results in the non-dimensional model

$$f_1^i = c_3 y_1^i \quad \text{and} \quad f_2^i = c_3 y_2^i,$$

in which $c_3 = kc/p_a Bd$.

Now consider the geometry at the trailing edge of the shell, in particular the rotation and compression of the spring. Let $T^i(X,T)$ denote the total distance from the surface of the shaft to the housing, $L^i(X)$ represent the distance from the shell to the housing before loading while still symmetric, ψ^i denote the anticlockwise rotation and $H^i(X,T)$ denote the film thickness at arclength X and time T. Then the compression at the trailing edge of the spring can be written

$$T^i(L,T) + Y_2^i + \left[2R_H \sin\left(\frac{\beta^i}{2}\right)\right] \psi^i = H^i(L,T) + L^i(L).$$

After non-dimensionalisation this equation becomes

$$h^i(R,t) = c_2^i + y_2^i + \phi^i, \tag{6}$$

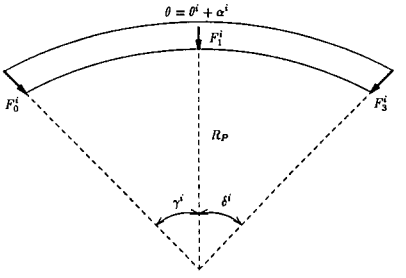

Fig. 3. Shell in a circular geometry.

where $c_2^i = [T^i(L,T) - L^i(L)]/c$, $H^i(L,T) = ch^i(R,t)$, $\phi_i = [2R_H \sin(\beta^i/2)]\psi^i/c$ and $Y_2^i = cy_2^i$. Similarly, at the leading edge of the spring

$$h^i(x',t) = c_1^i + y_1^i - \left[\frac{\sin(\alpha^i/2)}{\sin(\beta^i/2)}\right]\phi^i. \tag{7}$$

The terms c_1^i and c_2^i are expressed in terms of x_S, ξ^i, y_S and η^i as follows:

$$c_1^i = c_M + (x_S + \xi^i)\sin(\theta^i + \alpha^i) + (y_S + \eta^i)\cos(\theta^i + \alpha^i)$$

and

$$c_2^i = c_M + (x_S + \xi^i)\sin(\theta^i + \alpha^i - \delta^i) + (y_S + \eta^i)\cos(\theta^i + \alpha^i - \delta^i).$$

Here c_M is the non-dimensional mean clearance, defined as follows. Half the diametric clearance is the minimum distance from the surface of the journal to the shells before any component moves or deforms. The dimensional mean clearance is equal to half the diametric clearance plus half the step height:

$$C_M = \frac{\text{Diametric Clearance}}{2} + \frac{S}{2}$$

and the dimensionless mean clearance is $c_M = C_M/c$.

Let R_P be the radius of the pad, δ^i the angle subtended between trailing edge of the shell and leading spring arm and γ^i the angle subtended between leading spring arm and leading edge of the shell. The independent variable on each shell is the arclength x. The angle θ is related to the independent variable by

$$\theta = \left(\frac{-\gamma^i}{x'}\right)x + (\theta^i + \alpha^i + \gamma^i),$$

where $\alpha^i + \beta^i = \delta^i$, $\delta^i = \gamma^i(R - x')/x'$ and x' is the arclength coordinate of the position of leading spring arm contact. The film thickness is expressed in two parts, the first being the rigid body motion and the second the deformation. The film thickness satisfies the relation

$$h^i(x,t) = -w^i(x,t) + c_M + (x_S + \xi_t^i)\sin\theta + (y_S + \eta_t^i)\cos\theta, \tag{8}$$

where ξ_t^i and η_t^i represent the rigid body motions of the shell. ξ^i and η^i represent the unloaded position of the shell and are solutions of the equations:

$$-\frac{s}{2} = \xi^i \sin(\theta^i + \alpha^i - \delta^i) + \eta^i \cos(\theta^i + \alpha^i - \delta^i)$$

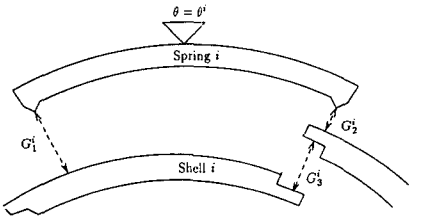

Fig. 4. Gaps that may occur in the conforming shell system.

and

$$\frac{s}{2} = \xi^i \sin(\theta^i + \alpha^i + \gamma^i) + \eta^i \cos(\theta^i + \alpha^i + \gamma^i),$$

where s is the non-dimensional step height.

After non-dimensionalisation by $F_0^i = p_a B f_0^i$, the moment equation becomes

$$f_1^i \sin(\delta^i) + f_0^i \sin(\gamma^i + \delta^i) = \int_0^R (p^i - 1) \sin(\theta - \alpha^i + \delta^i - \theta^i)\, \mathrm{d}x. \tag{9}$$

Resolving along the radius at $\theta = \theta^i + \alpha^i$ results in the second, and last, force equilibrium equation for the shell. (Note that the resolution equation perpendicular to the radius $\theta = \theta^i + \alpha^i$ can be derived from equations (9) and (10) providing $\cos\delta^i \neq 0$.) After the non-dimensionalisation by $F_3^i = p_a B f_3^i$, the resolution equation along $\theta = \theta^i + \alpha^i$ becomes

$$f_1^i + f_0^i \cos(\gamma^i) + f_3^i \cos(\delta^i) = \int_0^R (p^i - 1) \cos(\theta - \theta^i - \alpha^i)\, \mathrm{d}x. \tag{10}$$

The next stage is to deal with the inter-shell links. The forces between adjacent shells must balance, so for the N-shell model this gives

$$f_2^{i+1} - f_3^{i+1} = f_0^i. \tag{11}$$

Introduce the gap for shell i, now no longer in contact with shell $i-1$, G_3^i, see Fig. 4. This gap is non dimensionalised by $G_3^i = cg_3^i$. Then the step height equation can be written

$$h^{i-1}(0,t) = h^i(R,t) + s + g_3^i. \tag{12}$$

While the two shells remain in contact the zero gap equation, $g_3^i = 0$, closes the system of equations. But the inequality $f_3^i > 0$ must be satisfied simultaneously. If there is a gap present between the two shells then the zero force equation, $f_3^i = 0$, closes the system of equations, and the inequality $g_3^i \geqslant 0$ must be satisfied simultaneously. Hence there are two models for each shell. The exact point at which transitions between these two different possibilities takes place is not known a priori. For each model there is an extra inequality constraint which predicts the point of transition.

If a break occurs between spring i, shell i and shell $i-1$ then spring i no longer plays any part in the system behaviour. The rotation of spring i cannot be determined uniquely as it is no longer in contact with any shells. However, the position of the spring must be uniquely determined to deduce the point at which contact is regained. Introduce two new variables G_2^i, the gap between spring i and shell $i-1$, and G_1^i, the gap between spring i and shell i. Non-dimensionalise both variables as $G_2^i = cg_2^i$ and $C_1^i = cg_1^i$. To fix the value of the spring

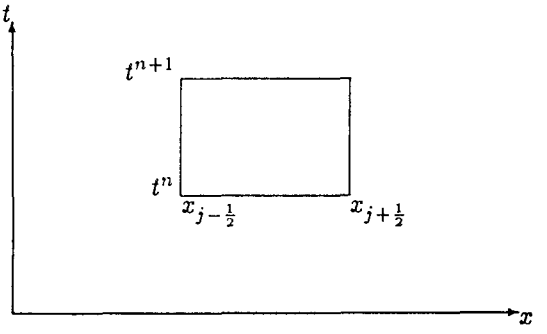

Fig. 5. Domain of integration in (x, t) space.

rotation assume that spring i is only just out of contact with shell $i-1$. That is, $0 < g_2^i \ll 1$ which to first order is the same as $g_2^i = 0$. Thus, the only new variable when a spring break occurs is g_1^i and as for the shell breaks this is determined by the equation $f_1^i = 0$. Thus, the film thickness at the leading edge of spring i is now given by

$$h^i(x', t) = c_1^i + y_1^i - \left[\frac{\sin(\alpha^i/2)}{\sin(\beta^i/2)}\right]\phi^i - g_1^i,$$

with the inequality $g_1^i \geqslant 0$. If contact is regained, $g_1^i = 0$ and the inequality $f_1^i > 0$ must be satisfied simultaneously. Hence there are two models for each spring i. The exact point at which transitions between these two different possibilities takes place is not known a priori.

Hence, ξ_t^i and η_t^i are given by

$$y_1^i - \left[\frac{\sin(\alpha^i/2)}{\sin(\beta^i/2)}\right]\phi^i - g_1^i = [\xi_t^i - \xi^i]\sin(\theta^i + \alpha^i) + [\eta_t^i - \eta^i]\cos(\theta^i + \alpha^i) \tag{13}$$

and

$$y_2^i + \phi^i - g_3^i = [\xi_t^i - \xi^i]\sin(\theta^i + \alpha^i - \delta^i) + [\eta_t^i - \eta^i]\cos(\theta^i + \alpha^i - \delta^i). \tag{14}$$

Equations (12), (13) and (14) are used to determine the angle of rotation of the spring and the two degrees of freedom of the shell. Equations (5), (9), (10) and (11) are the four equations employed to determine the forces per unit axial length. There are two possible equations to solve for each of the gaps either a zero force condition or a zero gap condition. This leads to a total of 4^N different models for an N-shell bearing each having to satisfy $2N$ additional inequality constraints. These $2N$ constraints on the solution space of each of the 4^N models determine the time at which transitions take place.

3. Numerical method

The Reynolds equation can be written in the following form:

$$f_x + w_t = 0,$$

where

$$f = \Lambda ph - ph^3\frac{\partial p}{\partial x} \qquad \text{and} \qquad w = \sigma ph.$$

Let x_j be a grid point and $x_{j+1/2} = (x_{j+1} + x_j)/2$. Integrating the Reynolds equation over a rectangular domain in (x, t) space as in Fig. 5 and applying Green's theorem,

$$\begin{aligned}\iint \{f_x + w_t)\,\mathrm{d}x\,\mathrm{d}t &= \int f\,\mathrm{d}t - w\,\mathrm{d}x \\ &\simeq (f^{n+\theta}_{j+\frac{1}{2}} - f^{n+\theta}_{j-\frac{1}{2}})(t^{n+1} - t^n) + (w^{n+1}_j - w^n_j)(x_{j+\frac{1}{2}} - x_{j-\frac{1}{2}}) \\ &= (f^{n+\theta}_{j+\frac{1}{2}} - f^{n+\theta}_{j-\frac{1}{2}})(t^{n+1} - t^n) + \frac{(w^{n+1}_j - w^n_j)(x_{j+1} - x_{j-1})}{2},\end{aligned}$$

where $f^{n+\theta}$ is an approximation to f between time levels. Our scheme is formed by setting the right-hand side to zero. By summing, we obtain the discrete conservation law:

$$\sum_{j=1}^{J-1} \frac{w^{n+1}_j (x_{j+1} - x_{j-1})}{2} = \sum_{j=1}^{J-1} \frac{w^n_j (x_{j+1} - x_{j-1})}{2} + (t^{n+1} - t^n)[f^{n+\theta}_{\frac{1}{2}} - f^{n+\theta}_{J-\frac{1}{2}}].$$

It is also sensible to suggest the following discretisation:

$$f_{j+\frac{1}{2}} \simeq \Lambda(ph)_{j+\frac{1}{2}} - (ph^3)_{j+\frac{1}{2}} \left(\frac{p_{j+1} - p_j}{x_{j+1} - x_j} \right).$$

As the Couette term (Λph) is induced by relative slide motion, we upwind this term:

$$\Lambda(ph)_{j+\frac{1}{2}} \simeq \Lambda(ph)_j.$$

The pressure gradient induces the Poiseuille term $(ph^3 \partial p/\partial x)$, so this is discretised symmetrically:

$$(ph^3)_{j+\frac{1}{2}} \simeq \frac{(ph^3)_{j+1} + (ph^3)_j}{2}.$$

The above is not the only possible symmetric discretisation. Others options include $(ph^3)_{j+\frac{1}{2}} = p_{j+\frac{1}{2}} h^3_{j+\frac{1}{2}}$ or even linear combinations of the above. However, we shall adopt the first choice. We discretise the term $f_{j-\frac{1}{2}}$ in a similar fashion. The functions $f^{n+\theta}$ can be interpreted as a weighted sum of f between the two different time levels t^n and t^{n+1}. This results in the following discretisation:

$$F^{n+\theta}_j = 0, \tag{15}$$

where

$$\begin{aligned}F^{n+\theta}_j &= \sigma((ph)^n_j - (ph)^{n+1}_j) + \theta \left\{ \frac{2(t^{n+1} - t^n)}{x_{j+1} - x_{j-1}} \right\} \\ &\quad \times \left(\Lambda(ph)_{j-1} - \Lambda(ph)_j + \left[\frac{(ph^3)_{j+1} + (ph^3)_j}{2} \right] \left(\frac{p_{j+1} - p_j}{x_{j+1} - x_j} \right) \right. \\ &\quad \left. - \left[\frac{(ph^3)_j + (ph^3)_{j-1}}{2} \right] \left(\frac{p_j - p_{j-1}}{x_j - x_{j-1}} \right) \right)^{n+1} + (1 - \theta) \left\{ \frac{2(t^{n+1} - t^n)}{x_{j+1} - x_{j-1}} \right\}\end{aligned}$$

$$\times\left(\Lambda(ph)_{j-1}-\Lambda(ph)_j+\left[\frac{(ph^3)_{j+1}+(ph^3)_j}{2}\right]\left(\frac{p_{j+1}-p_j}{x_{j+1}-x_j}\right)\right.$$
$$\left.-\left[\frac{(ph^3)_j+(ph^3)_{j-1}}{2}\right]\left(\frac{p_j-p_{j-1}}{x_j-x_{j-1}}\right)\right)^n$$

for $j=1,2,\ldots,J-1$. The boundary conditions for pressure are imposed in the form

$$p_0^n=p_J^n=1 \qquad \text{for all } n.$$

Equation (2), the curved beam equation, with appropriate boundary conditions is an Euler–Lagrange formulation of an extremum principle. The minimisation of strain energy in this extremum principle is an alternative physical statement of this problem. In particular, the corresponding variational problems can easily be solved using the finite element method, see [8] and [9]. The Sobolev space in which the solution for $w^i(x,t)$ is sought at time t is therefore

$$H_E^2=\{w^i(x)\in H^2(0,R)|w^i(x')=0, w^i(R)=0\}.$$

Thus, the weak formulation of this problem for $w^i|_{\{t=\text{constant}\}}\in H_E^2$ is

$$a(w^i,u)=l(u) \quad \text{for all } u\in H_E^2,$$

where the bilinear form

$$a(w^i,u)=\int_0^R r\left(\frac{\partial^2 w^i}{\partial x^2}\frac{\partial^2 u}{\partial x^2}-2\kappa^2\frac{\partial w^i}{\partial x}\frac{\partial u}{\partial x}+\kappa^4 u w^i\right)\mathrm{d}x$$
$$-r\kappa^2\left[u(0,t)\frac{\partial w^i}{\partial x}(0,t)+w^i(0,t)\frac{\partial u}{\partial x}(0,t)\right]$$

and the linear functional

$$l(u)=\int_0^R u(1-p)\,\mathrm{d}x+f_0^i u(0,t).$$

In the linear functional the term $r(\partial^3 w^i/\partial x^3+\kappa^2\partial w^i/\partial x)(0,t)$ is identified with the dimensionless force per unit axial length f_0^i. For the finite element space to be conforming it is necessary that members of the trail space have continuous first derivatives and the position of spring contact is chosen to be a mesh point. So the standard choice for this problem of Hermite cubic basis functions was made and the mesh chosen appropriately.

Consider equation (4), which may be rewritten as the system

$$\frac{\mathrm{d}v_S}{\mathrm{d}t}=\Gamma\sum_i\int_0^R p^i\cos(\theta)\,\mathrm{d}x+l$$

and

$$\frac{\mathrm{d}y_S}{\mathrm{d}t}=v_S.$$

Numerical methods to discretise ordinary differential equations of this type are described in [10]. Integrating both sides of these equations between t^n and t^{n+1} results in the equations

$$v_S(t^{n+1})=v_S(t^n)+\int_{t^n}^{t^{n+1}}\Gamma\sum_i\int_0^R p^i\cos(\theta)\,\mathrm{d}x\,\mathrm{d}t+l(t^{n+1}-t^n) \tag{16}$$

and

$$y_S(t^{n+1}) = y_S(t^n) + \int_{t^n}^{t^{n+1}} v_S \, dt. \tag{17}$$

It only remains to choose a discrete approximation to the integrals in time and space. The integral in space is approximated simply by the trapezium rule. However, the integral in time has already been considered in the discretisation of the Reynolds equation. It would be inconsistent to choose a different approximation to this operator at this point, so we use the weighted sum as before. Hence equations (16) and (17) are discretised as

$$v_S^{n+1} = v_S^n + l(t^{n+1} - t^n) + \theta(t^{n+1} - t^n)\Gamma \sum_i \sum_{r=0}^{J-1} \frac{(x_{r+1} - x_r)}{2} \mathcal{F}^i(x_r, x_{r+1})^{n+1}$$

$$+(1-\theta)(t^{n+1} - t^n)\Gamma \sum_i \sum_{r=0}^{J-1} \frac{(x_{r+1} - x_r)}{2} \mathcal{F}^i(x_r, x_{r+1})^n$$

and

$$y_S^{n+1} = y_S^n + (t^{n+1} - t^n)[\theta v_S^{n+1} + (1-\theta)v_S^n],$$

where

$$\mathcal{F}^i(x_r, x_{r+1}) = p^i(x_{r+1}, t)\cos\theta(x_{r+1}) + p^i(x_r, t)\cos\theta(x_r).$$

Similarly we discretise equation (3).

The integrals in the moment equations and resolution equations are estimated by the trapezium rule.

Three important points must be taken into account when choosing the spatial mesh. The first point is that there is a boundary layer at the trailing edge of the pressure profile. The second point is that the location of spring contact must be a mesh point if the trial space is to be conforming. The third is that for each extra mesh point there is an increase of $4N$ extra unknowns in the solution vector. The answer is clearly a mesh function which compromises between these requirements. The mesh should be clustered towards the trailing edge of the shells to capture the pressure change. The local clustering of points does not increase the number of mesh points excessively. Also the variation in mesh sizes must be continuous to ensure the truncation errors do not become large.

The discretisation so far simulates the full bearing without breaks, and the solution of this nonlinear algebraic system must be found at each time-step. Two methods were experimented with. The first was a Picard iteration taking the equations in turn and substituting the solution of one into the right-hand side of another, until no further changes took place. The second was a matrix method solving all the equations in one large Newton iteration.

The Picard iteration did not always converge, and when it converged it did so slowly. To attempt to remedy this situation numerical experiments with variable relaxation factors took place. This did guarantee convergence in most cases, although the convergence was slow.

The Jacobian in Newton's method is of the form

$$\begin{pmatrix} A & B \\ P & Q \end{pmatrix} \begin{pmatrix} \mathbf{x}_1 \\ \mathbf{x}_2 \end{pmatrix} = \begin{pmatrix} \mathbf{c} \\ \mathbf{d} \end{pmatrix},$$

where A is a banded square matrix. The upper section of the Jacobian contains the finite element discretisations, the algebraic equations for the film thickness and the linearisations

of the discretisation of the Reynolds equation. The lower section of the Jacobian contains integral equations for the forces, the algebraic equations for the rigid body motions and the discretisation of the system of ordinary differential equations in time representing the shaft motion. $\mathbf{x}_1$ is a vector of $4N(J+1)$ elements and $\mathbf{x}_2$ is a vector of $9N+4$ elements for an N-shell bearing with $(J+1)$ mesh points on each shell. The four unknowns on each mesh point are pressure, film thickness, deformation and the derivative of the deformation. There are also $4N$ unknown forces, $3N$ unknown rigid body motions, $2N$ unknown gaps, the position of the shaft and the velocity of the shaft. Alternatively, the matrix system can be written as the simultaneous equations

$$A\mathbf{x}_1 + B\mathbf{x}_2 = \mathbf{c}$$

and

$$P\mathbf{x}_1 + Q\mathbf{x}_2 = \mathbf{d},$$

where A is a square matrix with bandwidth thirteen. Thus

$$\mathbf{x}_1 = A^{-1}(\mathbf{c} - B\mathbf{x}_2) \tag{18}$$

and

$$(Q - PA^{-1}B)\mathbf{x}_2 = (\mathbf{d} - PA^{-1}\mathbf{c}). \tag{19}$$

To solve this system requires the following steps:

1. Solve $A\mathbf{z} = \mathbf{c}$
2. Solve $AW = B$
3. Solve equation (19) for $\mathbf{x}_2$
4. Solve equation (18) for $\mathbf{x}_1$

Clearly steps 3 and 4 are trivial; the only hard work is involved in inverting A. This is achieved by using a banded LU decomposition technique with partial pivoting which takes advantage of the structure of A and can be used on multiple right-hand sides. The matrix A is stored as column vectors, diagonally down the band, resulting in very low storage requirements.

The numerical treatment of separation relies on knowing which constraints are active at the previous time-step. Assume first of all that this set of constraints still applies over the next time-step. Process the next time-step and examine the feasibility of the solution. If the solution is feasible, then continue to the following time-step. However, if the solution is infeasible examine the solution vector. Rely on the assumptions that:

(a) A negative force indicates a break on the next time-step.

(b) A negative gap indicates contact regained on the next time-step.

Update the active set of constraints over the time-step and process the solution again. This process should continue until a feasible solution is obtained, or a maximum number of attempts to find a feasible solution have failed. The matrix method of solution naturally accepts the new equality constraints necessary for separation. The new equations affect P, Q and d only. The Picard iteration would require a multi-dimensional shooting technique to deal with separation. This is an additional reason to favour the matrix method over Picard iteration.

The discretisation can clearly be seen to be consistent with the model. The only difficulties are the time-steps where a transition takes place. During these time intervals the discretisation is inconsistent, but the total time interval is $O(Dt)$ where Dt is the time-step. By choosing a suitable degree of implicitness the scheme does not suffer from numerical instabilities.

There are numerical aspects of this problem that cannot be guarded against. These include the possibility that Newton's method is not provided with a good enough first guess. This situation can result in either an incorrect root of the nonlinear algebraic system being found or the iteration not converging at all. Newton's method can be aided considerably in these situations by reducing the time-step. Also there is no guarantee that the technique for finding feasible solutions will work. Indeed it has not been proved that a feasible solution to the algebraic system exists.

4. Results of the simulation

The different factors limiting the stable operation of the conforming shell bearing will be investigated here. These factors include dynamic instability and separations between bearing components. It is not feasible to perform a comprehensive study of all bearing designs, so a specific design will be chosen and reported upon.

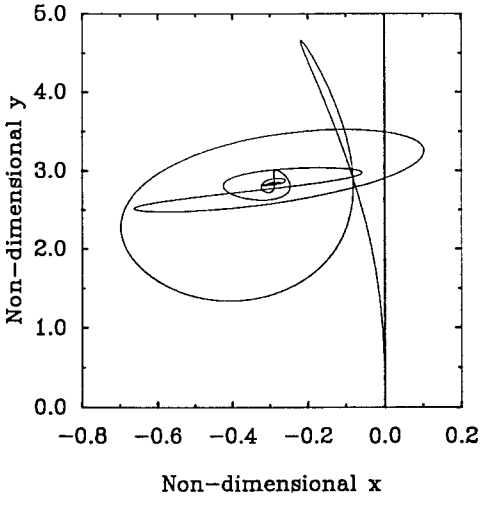

Fig. 6. Trajectory of the shaft centre for a 4-shell bearing with $l = 120$.

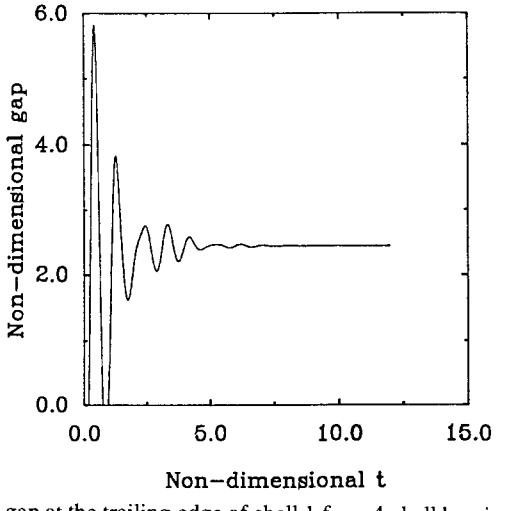

Fig. 7. Variation of gap at the trailing edge of shell 1 for a 4-shell bearing with $l = 120$.

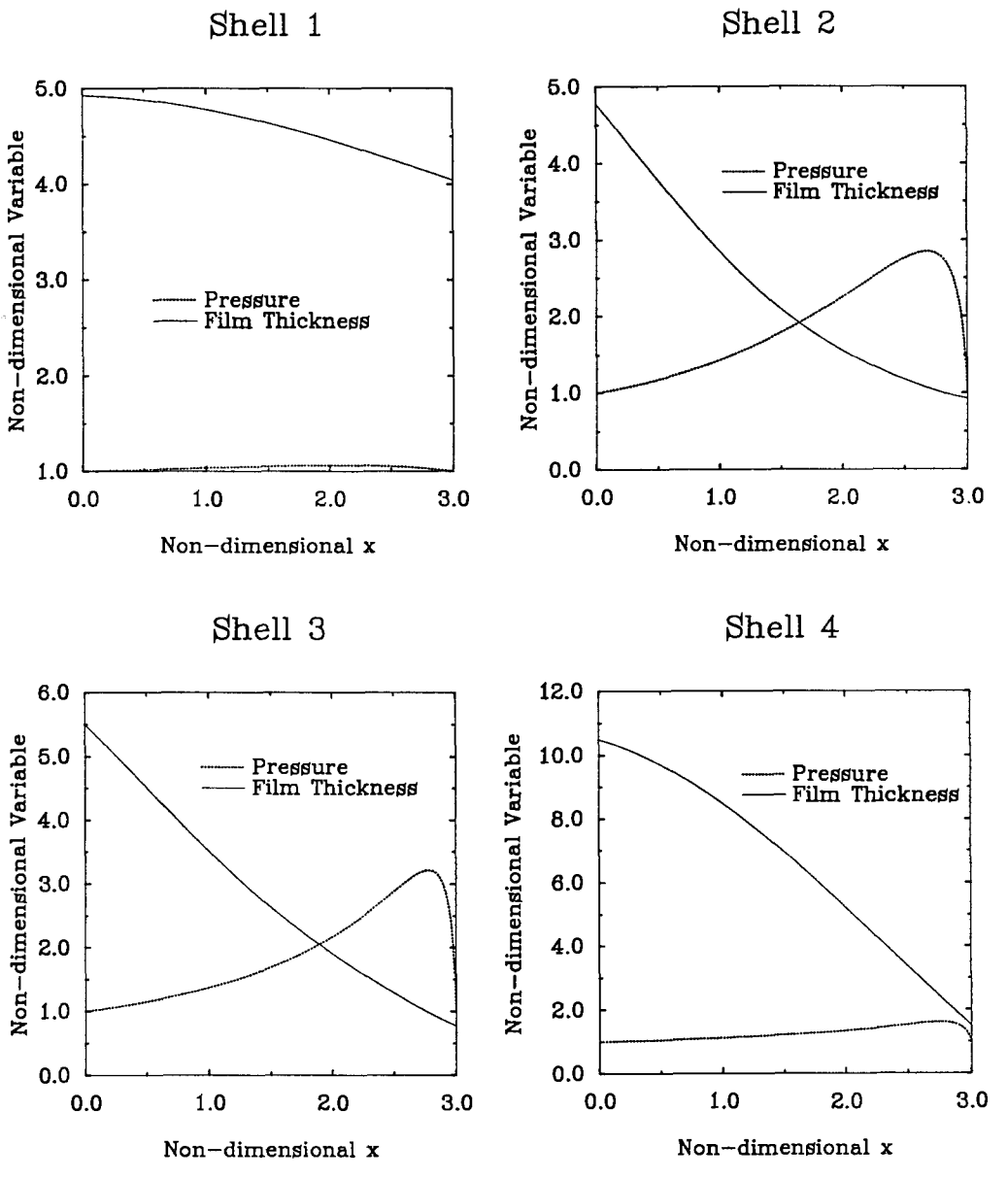

Fig. 8. Steady state results for a 4-shell bearing with $l = 120$.

Consider a 4-shell application where the shaft is started at the origin and allowed to time step until steady state is reached or a maximum number of steps have elapsed. Shells are labelled in an anti-clockwise direction starting from shell 1, see Fig. 1. The leading edge is always $x = 0.0$, the trailing edge in this case is $x = 3.0$. Let the y_S-axis be along the line of action of the applied load. The x_S-axis is taken perpendicular to the y_S-axis and through the centre of the housing, see Fig. 1. Hence the origin is the housing centre. The 4-shell bearing is as shown in Fig. 1. Choose the following parameter set:

$$\Lambda = 19, \quad \sigma = 1, \quad \Gamma = 40, \quad l = 120, \quad c_M = 4, \quad \kappa = 0.5, \quad r = 1,$$

$$s = 4, \quad c_3 = 4.2, \quad \theta^1 = 0.79, \quad \frac{\alpha}{\beta} = 0.43 \text{ and } \frac{\gamma}{\gamma + \delta} = 0.44.$$

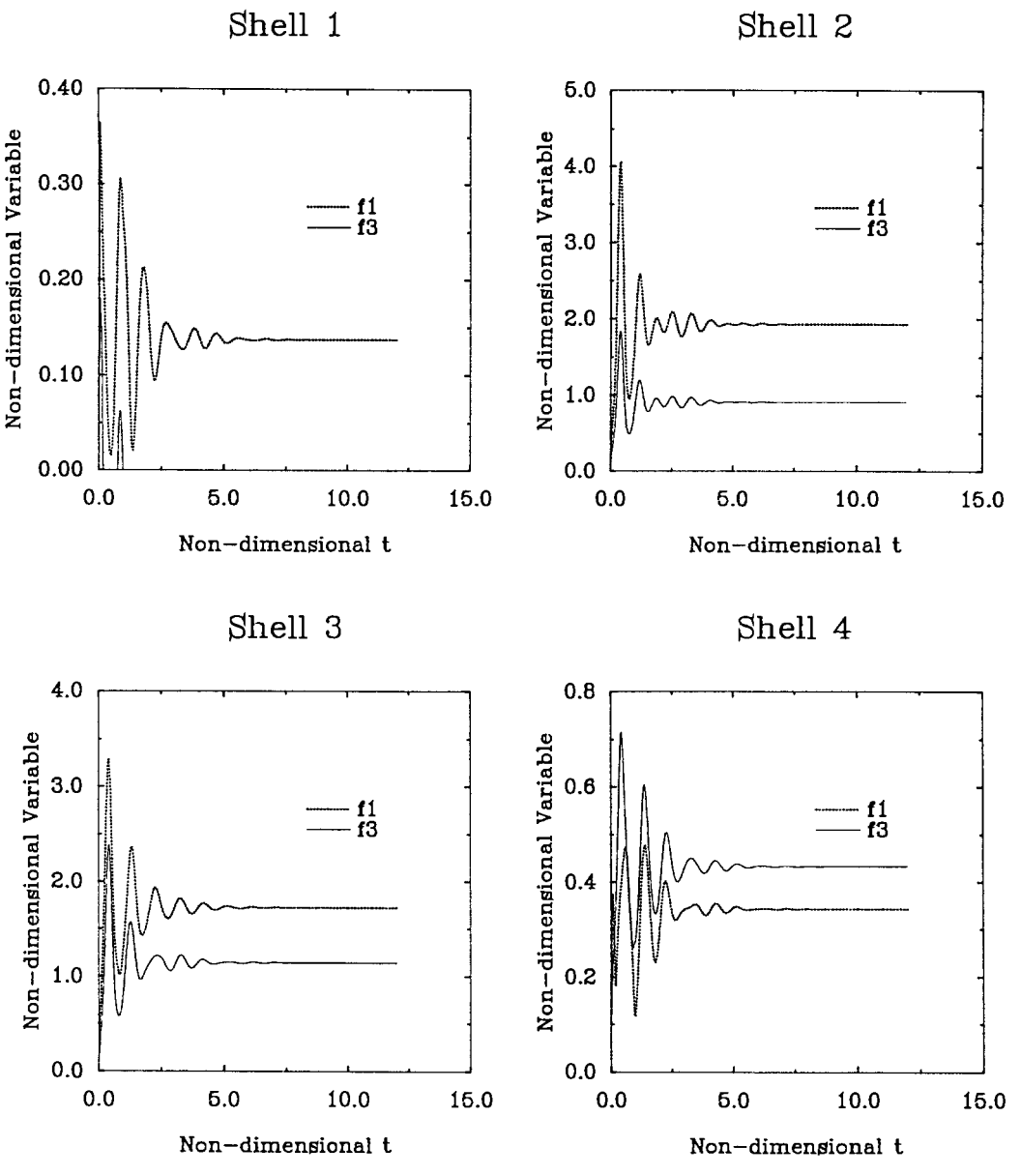

Fig. 9. Comparison of the variation of force with time for a 4-shell bearing with $l = 120$.

The definitions of these parameters are given in Appendix A for convenient reference. The time-step, for the results in this section, is chosen to be 0.002 with 40 space intervals on each shell. The steady state was characterised by the velocity of the shaft in both directions being zero to four decimal places.

The trajectory of the shaft centre is given in Fig. 6. The steady state profiles of pressure and film thickness are given in Fig. 8. Note that the pressure generated on shell 1 and shell 4 is insignificant in comparison to shell 2 and shell 3. The bottom two shells take all the load from the shaft. The parameter set is particularly interesting in that it gives rise to breaks in the conforming shell system. In Fig. 7 the variation of the gap at the trailing edge of shell 1

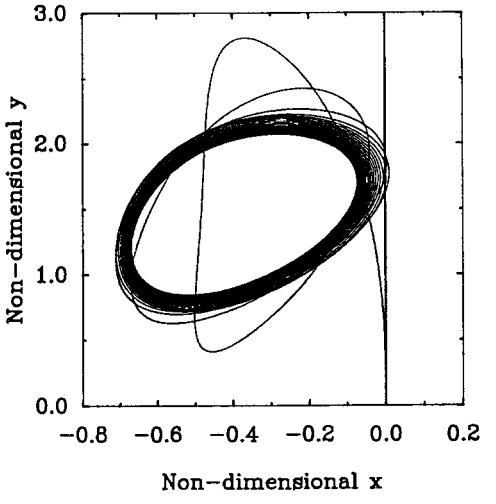

Fig. 10. Trajectory of the shaft centre for a 4-shell bearing with $l = 65$.

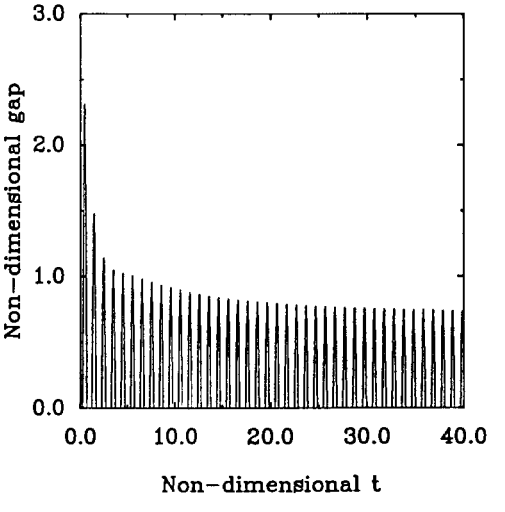

Fig. 11. Variation of gap at the trailing edge of shell 1 for a 4-shell bearing with $l = 65$.

against time can be observed. It is of value to compare this gap with the variation of f_3 on shell 1 in Fig. 9. Notice that the gap is zero when the force is positive and vice versa.

Load in itself is seen as a stabilizing influence when all other properties remain constant. This stabilizing is well-known in the engineering literature [1]. Thus, reducing l might well reveal other characteristics of this design. Keeping the parameter set from the first run except putting $l = 65$ produces the trajectory in Fig. 10 after 20000 time-steps. The orbit in Fig. 10 decreases in amplitude as time progresses, but the rate of reduction gets progressively slower. This orbit is either just stable or producing a limit cycle. Experimental evidence does indicate that periodic orbits do occur in rotating machinery. However, as they usually occur very close

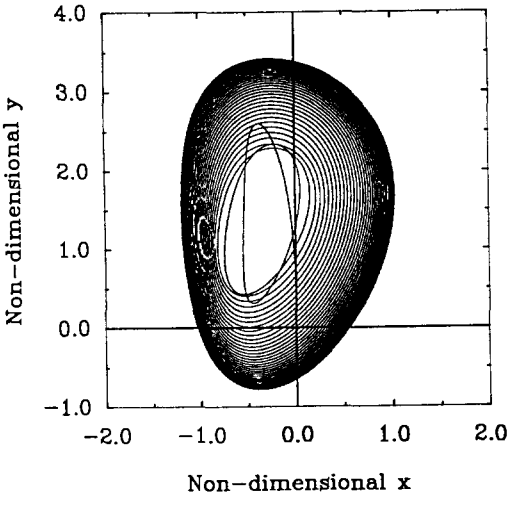

Fig. 12. Trajectory of the shaft centre for a 4-shell bearing with $l = 60$.

to the onset of destructive instabilities, they are costly to investigate. It is very difficult to predict whether the orbit in Fig. 10 is in fact tending to a periodic orbit or just slowly tending to an equilibrium point. Moreover the accompanying graph in Fig. 11 for this parameter set reveals the very worrying characteristic of chatter. Chatter is the rapid intermittent contact between components which is very likely to cause damage. However, this particular effect is present only for parameter sets that are already periodic, so it is not a further restriction.

If the load is reduced slightly further major changes occur in the trajectories of the shaft. Keeping the same parameter set as the first run except putting $l = 60$ produces the trajectory in Fig. 12 after 20000 time steps. The orbit in Fig. 12 is increasing in amplitude as time progresses, and the rate of increase is getting progressively slower. This behaviour represents either an unstable orbit or a limit cycle.

There are other solution techniques which, although limited in their region of application, can be used to check the numerical results. Analytical solutions to the Reynolds equation and beam equation can be found to check the discretisations individually. Also asymptotic techniques [11] can be used to construct simplified systems.

5. Conclusions

The main objective of this investigation was to gain understanding of the dynamic and steady behaviour of the conforming shell gas journal bearing. It turns out that there are three factors limiting the operation of the bearing. The first factor is the onset of dynamic instabilities. The second factor is the possibility of touchdown during the start-up phase of operation. The third factor is separations. For any particular design these factors form the upper and lower bounds on the range of acceptable loads. In conclusion, this analysis predicts that this design can operate at the higher loads, speeds and temperatures required.

A. Index of Dimensionless Constants

Description	Formula	Symbol
bearing number	$6\mu UB/p_a c^2$	Λ
squeeze number	$12\mu B^2\nu/p_a c^2$	σ
flexibility coefficient in beam equation	$EIc/p_a dB^4$	r
curvature coefficient in beam equation	B/Rp	κ
dimensionless length of the shell	L/B	R
dimensionless spring coefficient	$kc/p_a Bd$	c_3
dimensionless coefficient in equation of journal	$p_a B/Mc\nu^2$	Γ
dimensionless load in equation of journal	$W_L/Mc\nu^2$	l
dimensionless step height	S/c	s
dimensionless mean clearance	$(\text{D.C.} + S)/2c$	c_M

Acknowledgment

Financial support for this work was provided by the Science and Engineering Research Council of Great Britain and Rolls-Royce plc. This project has benefited from the generous advice of P. Withers, T. V. Jones and S. I. Hogg.

References

1. V. Castelli and H. G. Elrod, Solution of the stability problem for 360 degree self-acting, gas-lubricated bearings. *Journal of Basic Engineering, Trans. ASME, Series D* 87 (1965) 99–212.
2. V. Castelli and J. T. McCabe, Transient dynamics of a tilting pad gas bearing system. *J. Lubrication Technology, Trans ASME, Series F* 89 (1967) 499–509.
3. A. Cameron, *Basic Lubrication Theory*. Chichester: Ellis Horwood (1976) 195 pp.
4. A. Burgdorfer, The influence of the molecular mean free path on the performance of hydrodynamic gas lubricated bearings. *Journal of Basic Engineering, Trans. ASME, Series D* 81 (1959) 94–100.
5. W. A. Gross, *Gas Film Lubrication*. New York: John Wiley & Sons (1962) 413 pp.
6. S. I. Hogg, T. V. Jones, A. Baker and P. Withers, Two-dimensional effects in gas dynamic journal bearings. *International Society for Airbreathing Engines* 2 (1989) 749–756.
7. A. Blake, *Handbook of Material Sciences and Structures*. New York: John Wiley & Sons (1985) 710 pp.
8. P. E. Lewis and J. P. Ward, *The Finite Element Method: principles and applications*. Amsterdam: Addison Wesley (1991) 421 pp.
9. D. S. Burnett, *Finite Element Analysis*. Amsterdam: Addison Wesley (1973) 844 pp.
10. J. D. Lambert, *Computational Methods in Ordinary Differential Equations*. London: John Wiley & Sons Ltd. (1973) 278 pp.
11. F. F. Ling, Asymptotic analyses in isothermal fluid film lubrication theories. *SIAM Review* 28 (1986) 343–366.